Macromolecules

Article

pubs.acs.org/Macromolecules

Trilayered Single Crystals with Epitaxial Growth in Poly(ethylene oxide)-*block*-poly(ε-caprolactone)-*block*-poly(L-lactide) Thin Films

Yeo-Wan Chiang,* You-Yuan Hu, Jhen-Ning Li, Shih-Hung Huang, and Shiao-Wei Kuo

Department of Materials and Optoelectronic Science, Center for Nanoscience and Nanotechnology, National Sun Yat-Sen University, Kaohsiung 80424, Taiwan

Supporting Information

ABSTRACT: Manipulation of crystalline textures of biocompatible block copolymers is critical for the applications in the medical field. Here, we present the control of multiple-crystalline morphologies with flat-on chain orientation in biocompatible poly(ethylene oxide)-*block*-poly(ε-caprolactone)-*block*-poly(L-lactide) (PEO−PCL−PLLA) triblock copolymer thin films using melt and solvent-induced crystallizations. Only single-crystalline morphologies of the first-crystallized blocks can be obtained in the melt-crystallized thin films due to the confinement effect. With solvent annealing by PCL-selective toluene, single-crystalline PLLA to double-crystalline PLLA/PCL and to triple-crystalline PLLA/PCL/PEO layered crystals in sequence are observed for the first time. With the control of solvent selectivity, different sequential crystallization involving first-crystallized PCL transferring to double-crystalline PCL/PLLA is obtained using PEO-selective *n*-hexanol for annealing. Surprisingly, the crystalline growth of the trilayered single crystal exhibits specific layer-by-layer epitaxial relationship. As a result, the multiple-crystalline textures of the PEO−PCL−PLLA thin films can be carried out by controlling solvent and polymer interaction.

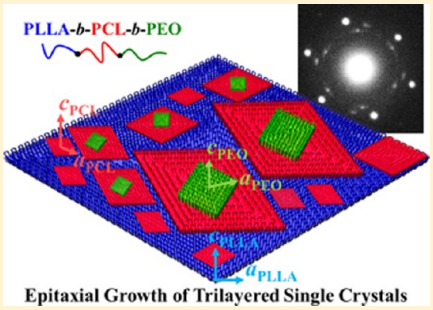

INTRODUCTION

Crystallization in block copolymers (BCP) has been drawn intensive attention because of the capability in the control of mechanical, biodegradable, biocompatible, and optoelectronic properties.[1−6] Morphologies and the corresponding crystal structures of semicrystalline BCPs consisting of a crystalline block and an amorphous block have been well studied,[7−16] which can give crystalline templates for material dispersions.[17−19] Recently, double-crystalline BCPs possessing two crystallizable blocks[20] such as poly(ethylene oxide)-*block*-poly(ε-caprolactone) (PEO−PCL),[21−23] poly(L-lactide)-*block*-poly(ε-caprolactone) (PLLA−PCL),[21−24] poly(L-lactide)-*block*-poly(ethylene oxide) (PLLA−PEO),[28−30] and poly(*p*-dioxanone)-*block*-poly(ε-caprolactone) (PPDX−PCL)[31,32] were extensively investigated due to their potential applications in the medical fields.[33−36] For the crystallization in the double-crystalline BCPs, when the crystallization temperatures of both blocks are similar such as PEO−PCL, the coincident crystallization for the two blocks is obtained. When the crystallization temperature for one of the crystallizable blocks is remarkably different from the other such as PLLA−PCL and PLLA−PEO, various crystalline conditions including one-stage and two-stage crystallizations can be conducted through the control of the crystallization sequence. Accordingly, the interactive crystallization of the crystalline blocks gives rise to diverse crystalline morphologies in double-crystalline BCPs. Some reports focused on the thin film crystallization of the double-crystalline BCPs.[37] For instance, Sun and co-workers reported that the first-crystallized PLLA single crystal constructed a one-dimensional confined environment for the subsequent crystallization of the PEO blocks in the PLLA−PEO BCPs, resulting in the unchanged lozenge-shaped PLLA morphologies including with PEG crystals.[28] Yang and co-workers found that that the foregoing crystallization of the PLLA block mainly determined the final morphologies in PLLA−PEO BCPs using melt crystallization, giving rise to the single crystals with lozenge-spiral dislocation, lozenges, and hexagonal multilayers.[29] Different from the polyester copolymers, Wang and co-workers studied the poly(3-butylthiophene)-*block*-polyethylene (P3BT−PE) BCPs and found that the surfaces of the lozenge PE crystals are covered with the P3BT layers to form the specific sandwiched morphology.[38]

It is well-known that triblock copolymers are able to self-assemble into various microphase-separated phases which are significantly distinct from the typical phases found in diblock copolymers. Because of the difficulty in the synthesis of triblock copolymers, few studies about the crystallization effect on the self-assembled morphologies of the triblock copolymers were reported especially for triple-crystalline block copolymers.[39] In contrast to the diblock copolymers, the constituted sequence of the building blocks can also be discussed in the triple-crystalline BCPs. In this study, thin film crystallization of biocompatible poly(ethylene oxide)-*block*-poly(ε-caprolactone)-*block*-poly(L-lactide) (PEO−PCL−PLLA)[40] BCPs consisting of three

Received: September 15, 2015
Revised: November 2, 2015
Published: November 23, 2015

DOI: 10.1021/acs.macromol.5b02042
Macromolecules 2015, 48, 8526−8533

Table 1. Characterization of the Block Copolymers

sample	$M_{n,PEO}$ (g/mol)	$M_{n,PCL}$ (g/mol)	$M_{n,PLLA}$ (g/mol)	$M_{n,total}$ (g/mol)	f_{PEO}^{v}	f_{PCL}^{v}	PDI
PEO5-PCL3-PLLA1	5400	2600	1000	9000	0.60	0.32	1.21
PEO5-PCL3-PLLA6	5400	2600	6300	14300	0.38	0.20	1.24

distinct crystallizable blocks was first explored using melt and solvent-induced crystallizations. Owing to the significant differences in the melting, crystallization temperatures, and glass transition temperatures, the sequential crystallization, coincident crystallization, and confined crystallization can be carried out in the PEO−PCL−PLLA. Also, the crystallization of the terminal PLLA block can be first conducted from the melt. Because of the similar crystallization window for the PEO and PCL blocks, the subsequent coincident crystallization of the PEO and PCL may give rise to diverse crystalline morphologies. Here, we found that only single-crystalline morphology of the first-crystallized block can be obtained in the melt-crystallized PEO−PCL−PLLA thin film. Interestingly, utilizing solvent-induced crystallization leads the PEO−PCL−PLLA thin film to successfully form multiple-crystalline morphologies including single-, double, and triple-crystalline layered crystals with flat-on chain orientation. The development of the layer-by-layer single crystals via epitaxial growth was also discussed.

EXPERIMENTAL SECTION

Materials and Sample Preparation. Poly(ethylene oxide)-*block*-poly(ε-caprolactone)-*block*-poly(L-lactide) (PEO-PCL-PLLA) block copolymers were prepared through the ring-opening polymerization (ROP) of L-lactide (LA, Aldrich) by hydroxyl-terminated PEO−PCL diblock copolymers purchased from Polymer Source Inc. The detailed synthesis was reported in the previous paper.[40] On the basis of molecular weight and volume fraction, the PEO-PCL-PLLA BCPs are assigned as PEO*x*-PCL*y*-PLLA*z* in which *x*, *y*, and *z* represent the molecular weights (kg/mol) of PEO, PCL, and PLLA blocks, respectively. The volume fractions of the PEO and PCL blocks are calculated by assuming that the densities of PEO, PCL, and PLLA are 1.12, 1.09, and 1.25 g/cm^3, respectively (see Table 1). Thin film samples of the BCPs were spun-cast on carbon-coated substrates at a rate of 1500 rpm from chlorobenzene (C_6H_5Cl) solutions (0.5 wt %). The as-spun thin films were further dried in a vacuum oven for 12 h at room temperature to remove the residual solvents.

***In Situ* Wide-Angle X-ray Diffraction (WAXD).** *In situ* WAXD experiments were conducted at the synchrotron X-ray beamline 23A at the National Synchrotron Research Center (NSRRC) in Taiwan. The wavelength λ of the X-ray beam was 0.2066 nm. A two-dimensional (2D) flat panel detector (C9728DK-10, Hamamatsu Japan) was used for collecting the 2D WAXD patterns. One-dimensional (1D) WAXD profiles were obtained by azimuthal integration of the 2D WAXD patterns. The positions of the diffraction peaks observed from WAXD experiments were carefully calibrated with silicon powder.

Transmission Electron Microscopy (TEM). A bulk sample of the PEO5-PCL3-PLLA6 was prepared by solution casting from dichloromethane solution (10 wt %) at room temperature for 2 days and was dried in a vacuum oven for 1 day to remove the residual solvent. The bulk sample was cryo-microtomed at −120 °C using a Reichert Ulracut microtome equipped with a Reichert FCS cyrochamber and a diamond knife. Staining was accomplished by exposing the microsections to the vapor of a 4% aqueous RuO_4 solution for 20 min. Bright-field TEM images employing mass−thickness contrast were obtained from the stained and Pt-shadowed samples on a JEOL JEM-2100 TEM at an accelerating voltage of 200 kV. After staining by RuO_4 vapor, the PEO microdomains are dark and the PCL as well as PLLA microdomains appear bright due to the enhanced difference of the mass−thickness contrast by preferential RuO_4 staining the PEO blocks.

Differential Scanning Calorimetry (DSC). For the nonisothermal crystallization, the samples were first heated to 160 °C for 3 min and then cooled to −50 °C at a rate of 10 °C/min using a PerkinElmer DSC7 equipped with an intracooler. For isothermal crystallization, the samples were first heated to 160 °C for 3 min and then rapidly cooled to the preset crystallization temperature at a rate of 150 °C/min. Each of the sample weight was 5 mg in all treatments of DSC. The melting temperature, T_m, was recorded by a scanning rate of 10 °C/min. The melting temperatures and endotherms were carefully calibrated using standard materials.

RESULTS AND DISCUSSION

Crystallization and Melting Sequences of Triple-Crystalline Block Copolymers. The crystallization behaviors of the PEO5-PCL3-PLLA1 and PEO5-PCL3-PLLA6 were explored using DSC. The bulk sample of the PEO5-PCL3-PLLA1 triblock copolymer was first heated to 160 °C for 3 min to erase the thermal history from solution casting and then cooled to −50 °C at a rate of 10 °C/min for nonisothermal crystallization. In Figure 1a, the DSC profile of the PEO5-PCL3-PLLA1 shows that two distinct temperatures of maximum crystallization rates (T_cs) can be found at 22.8 and 8.1 °C, respectively. Also, the DSC heating thermogram displays two melting temperatures (T_ms) at 45.2 and 51.3 °C in the subsequent heating process. The corresponding wide-angle X-ray diffraction (WAXD) profile (Figure S1a) only reveals the reflections of the PEO and PCL crystals. Therefore, the observed two melting peaks result from the PEO and PCL crystallizations. Moreover, no PLLA melting peaks can be obtained in the sample after long-time annealing at 50−100 °C. The absence of the characteristic reflections of the PLLA indicates the noncrystalline PLLA in the PEO5-PCL3-PLLA1 due to the low M_w of the PLLA block. In contrast, the DSC profile of the PEO5-PCL3-PLLA6 exhibits various T_cs at 73.2, 15.7, and 5.4 °C during cooling (Figure 1b). The subsequent heating profile displays various T_ms at 48.4, 51.8, and 134.4 °C. In accordance with the corresponding WAXD profile (Figure S1b), the characteristic reflections of the PCL, PEO, and PLLA crystals are all observed, indicating the triple-crystalline feature in the PEO5-PCL3-PLLA6. In contrast to the PEO5-PCL3-

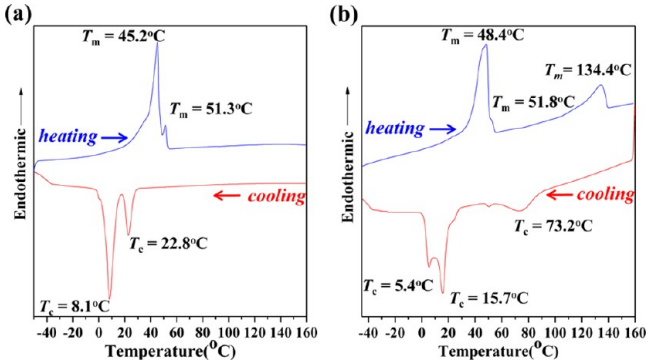

Figure 1. DSC heating (upper) and cooling (lower) profiles of the (a) PEO5-PCL3-PLLA1 and (b) PEO5-PCL3-PLLA6. The cooling and heating rates are 10 °C/min.

DOI: 10.1021/acs.macromol.5b02042
Macromolecules 2015, 48, 8526−8533

PLLA1, the increase of the PLLA chain length in the PEO5-PCL3-PLLA6 gives rise to stronger incompatibility from the adjacent PCL block chains, leading to the crystallizable PLLA.

To identify the crystallization sequence of the PEO5-PCL3-PLLA6, the *in situ* WAXD experiments were performed. In Figure 2a, the unstructured WAXD profile at 160 °C reveals the

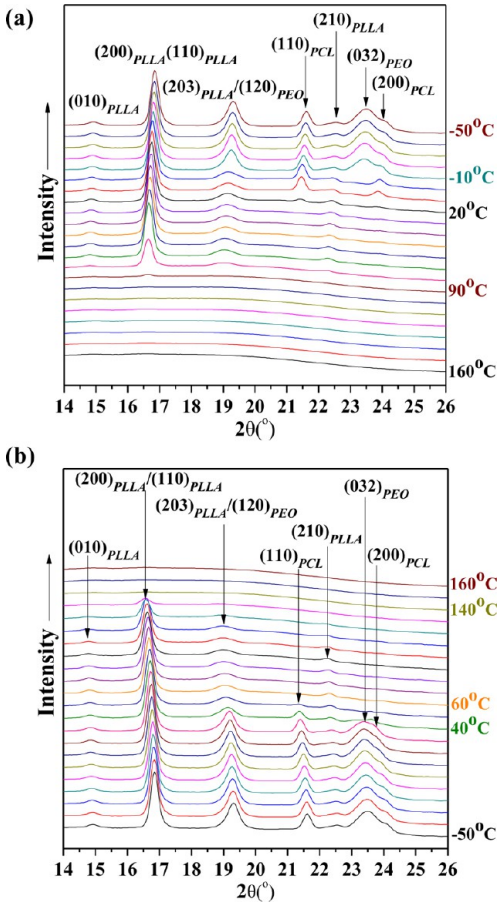

Figure 2. *In situ* WAXD profiles of the PEO5-PCL3-PLLA6 (a) cooled from 160 to −50 °C and (b) subsequently heated from −50 to 160 °C at a rate of 10 °C/min. Each temperature step is 10 °C.

amorphous PEO-PCL-PLLA in the melt state. During cooling at 90 °C, the reflection at $2\theta = 16.7°$ belonging to the $(110)_{PLLA}$ and $(200)_{PLLA}$ is obtained, indicating that PLLA is the first-crystallized block from the melt. At 20 °C, a new reflection of $(110)_{PCL}$ at $2\theta = 21.4°$ is found, indicating the second-crystallized PCL block. The third-crystallized PEO is demonstrated at −10 °C in accordance with the appearance of the $(032)_{PEO}$ reflection at $2\theta = 23.4°$ and the dramatically enhanced intensity at $2\theta = 19.3°$ by the $(120)_{PEO}$ reflection. Accordingly, the T_cs of the PLLA, PCL and PEO blocks are 90, 20, and −10 °C, respectively. The crystallization sequence of the PEO5-PCL3-PLLA6 cooled from the melt can be thus identified, i.e., $T_{c,PLLA} > T_{c,PCL} > T_{c,PEO}$. The discrepancy between the DSC and *in situ* WAXD results is attributed to the difference in the size of the sample chamber. Also, the complicated melting behavior of the PEO5-PCL3-PLLA6 can be examined by the *in situ* WAXD experiment during the subsequent heating process. As shown in Figure 2b, the $(120)_{PEO}$, $(200)_{PCL}$, and $(110)_{PLLA}/(200)_{PLLA}$ reflections disappear at 40, 60, and 140 °C, respectively. This expresses the melting sequence that the first-melting crystal is the PEO crystallite followed by the PCL and PLLA crystallites, i.e., $T_{m,PLLA} > T_{m,PCL} > T_{m,PEO}$. As a result, the crystallization and melting sequences of the PEO5-PCL3-PLLA6 can be clearly identified.

Microphase Separation of Triblock Copolymers. In Figure 3a, the small-angle X-ray scattering (SAXS) profile

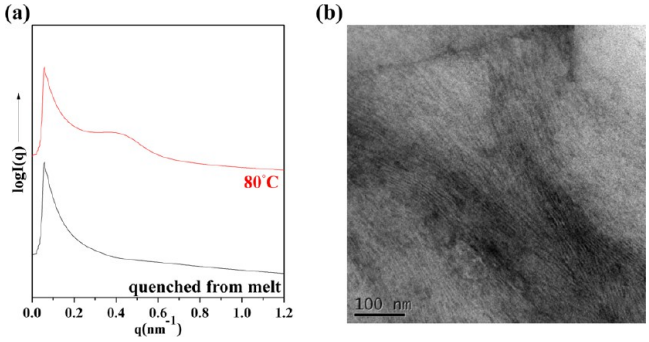

Figure 3. 1-D SAXS profile and TEM micrograph of the PEO5-PCL3-PLLA6. After RuO_4 staining, the dark region is PEO, and bright region is PCL and PLLA.

shows that no scattering peak can be obtained in the PEO5-PCL3-PLLA6 after quenched from the melt. In accordance with the corresponding WAXD profile (Figure S2), only PEO and PCL are crystalline in the PEO5-PCL3-PLLA6. Because of the similar electron densities for the amorphous PLLA (ρ^a_{PLLA} = 396 e/nm^3), crystalline PCL (ρ^c_{PCL} = 393 e/nm^3), and crystalline PEO (ρ^c_{PEO} = 400 e/nm^3),[41−43] the insignificant contrast of the scattering length density (SLD) results in the unstructured profile. When the sample was heated to 80 °C, in which PLLA crystallizes but PEO and PCL were melted, a broad scattering peak at the q value of 0.42 nm^{-1} can be found. This is attributed to the enlargement of the SLD contrast based on the values of the electron densities of the crystalline PLLA (ρ^c_{PLLA} = 410 e/nm^3), amorphous PCL (ρ^a_{PCL} = 354 e/nm^3), and amorphous PEO (ρ^a_{PEO} = 360 e/nm^3). The broad scattering peak at 80 °C suggests the breakout morphology by the PLLA crystallization under soft confinement. Since it is incapable of acquiring the morphological information on the PEO5-PCL3-PLLA6 using SAXS, we thus explored the microphase separation using transmission electron microscopy (TEM). As shown in Figure 3b, the lamellar morphology can be observed in the PEO5-PCL3-PLLA6 after being quenched from the melt. Owing to the coexistence of the PCL and PEO crystals, this lamellar morphology is the consequence of crystallization-driven microphase separation by the PCL and PEO crystallites.

Melt Crystallization of BCP Thin Films. In contrast to solution crystallization (i.e., crystal growth in a dilute solution), melt crystallization can provide a convenient way to form a solid crystalline texture in thin film for the practical applications. The BCP thin film was fabricated by spin-casting from a chlorobenzene solution (0.5 wt %) on a carbon-coated glass substrate and was then dried in a vacuum oven at room temperature for 12 h. The thin film was first heated to 170 °C for 3 min and was subsequently cooled to a preset temperature (T_{iso}) for isothermal crystallization. After isothermal crystallization, the thin film was finally quenched to room temperature for morphological investigation, namely, one-step crystallization (i.e., a single T_{iso}). Figure 4 shows the morphologies and the corresponding selected area electron diffraction (SAED)

DOI: 10.1021/acs.macromol.5b02042
Macromolecules 2015, 48, 8526−8533

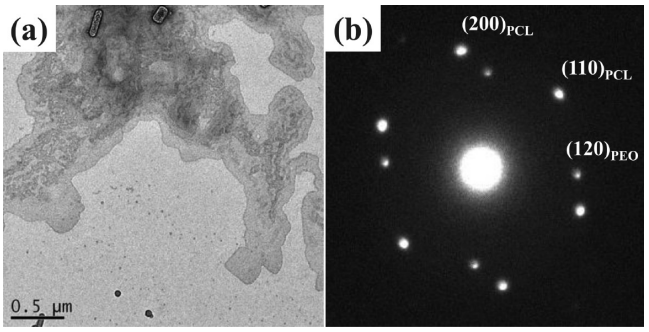

Figure 4. (a) TEM micrograph and (b) the corresponding SAED pattern of the PEO5-PCL3-PLLA1 crystallized at 45 °C for 3 h.

patterns of the PEO5-PCL3-PLLA1 thin films after melt crystallization at T_{iso} = 45 °C. As shown in Figure 4a, featureless crystalline morphology can be observed under TEM. The corresponding SAED pattern displays ten reflections belonging to the characteristic reflections of the PCL and PEO crystals (Figure 4b). Based on the monoclinic lattice structure of the PEO crystal (a = 0.805 nm, b = 1.304 nm, c = 1.948 nm and $\alpha = \gamma = 90°$, $\beta = 125.4°$)[44] and the orthorhombic lattice structure of the PCL crystal (a = 0.747 nm, b = 0.498 nm, c = 1.705 nm and $\alpha = \beta = \gamma = 90°$),[45] the inner four spots result from to the $(120)_{PEO}$ reflections and the outer six spots are attributed to the $(200)_{PCL}$ and $(110)_{PCL}$ reflections. These [001] zonal reflections indicate the coexistence of the flat-on PCL and PEO single crystals. Namely, both c-axes of the PEO and PCL crystals are perpendicular to the substrate surface (or parallel to the substrate normal). Consequently, this indicates the formation of the dual-layered PCL/PEO single crystals. Notably, the shape of the single crystals in the PEO5-PCL3-PLLA1 is irregular. This is due to the disruption of the amorphous PLLA block chains and the competitive coincident crystallization for the PEO and PCL blocks.

Figure 5 shows the TEM micrographs and the corresponding SAED patterns of the PEO5-PCL3-PLLA6 thin films after melt crystallization at various T_{iso}s. In Figure 5a, the lozenge-shaped single crystal with spiral growth is obtained at T_{iso} = 90 °C. According to the orthorhombic α-form PLLA crystal (a = 1.07 nm, b = 0.595 nm, c = 2.78 nm and $\alpha = \beta = \gamma = 90°$),[46,47] the six spots belong to the $(200)_{PLLA}$ and $(110)_{PLLA}$ reflections, revealing the formation of the flat-on PLLA single crystal. At T_{iso} = 45 °C, the featureless crystalline morphology is observed (Figure 5b). The corresponding six reflections of the $(200)_{PCL}$ and $(110)_{PCL}$ indicate the formation of the flat-on PCL single crystal. In contrast to the well-defined PLLA single crystal at T_{iso} = 90 °C, the featureless PCL single crystals at T_{iso} = 45 °C is due to the obstruction of the vitrified PLLA blocks (glass transition temperature of PLLA ∼ 50 °C). Similarly, the featureless PEO single crystal is found at T_{iso} = −10 °C (Figure 5c). It is noticed that unlike the PEO crystal having flat-on c-axis at T_{iso} = 45 °C in the PEO5-PCL3-PLLA1, the observed two $(120)_{PEO}$ reflections indicated the formation of the edge-on (i.e., the c-axis is parallel to the substrate surface) PEO single crystal. As reported by Zhu and co-workers,[48] the chain orientation of the PEO crystal could transfer from flat-on to edge-on orientations with the decrease of the crystallization temperature. Accordingly, the observed edge-on PEO crystal is attributed to the low crystallization temperature (T_{iso} = −10 °C). As a result, single-crystalline textures including flat-on PLLA, flat-on PCL, and edge-on PEO single crystals were obtained in the PEO5-PCL3-PLLA6 thin films after one-step melt crystallization even though these thin films were finally quenched to room temperature (∼25 °C) which is typically suitable for the crystal growth of the PCL. Similarly, only single-crystalline morphologies could be observed in the PEO5-PCL3-PLLA6 thin films after two-step (such as 90 °C → 45 °C, 90 °C → −10 °C, 45 °C → −10 °C or −10 °C → 45 °C) (Figures S3−S6) or three-step melt crystallization (such as 90 °C → 45 °C → −10 °C) (Figure S7). All of them displayed the single crystals directed by the first-crystallized blocks. We suggest that the first-crystallized event can drive the exclusion of the amorphous blocks onto the surfaces of the first-crystallized single crystal, resulting in the restriction of the chain mobility of the exclusive block chains. The subsequent crystallization is thus suppressed by the confined environment of the first-crystallized single crystal. As a result, the first-crystallized event mainly determines the final crystalline morphologies of the melt-crystallized PEO5-PCL3-PLLA6 thin films.

Solvent-Induced Crystallization of BCP Thin Films. To improve the chain mobility and acquire multiple-crystalline morphologies, we thus performed solvent-induced crystallization. The as-spun thin films were exposed under different solvent vapors such as toluene and n-hexanol for different time periods. Prior to solvent annealing, the PEO5-PCL3-PLLA6 thin film spun-cast from the chlorobenzene solution displays flat-on PCL single crystals as evidenced by the weak [001] zonal reflections (Figure S8). Also, the probability to obtain the diffraction patterns from the PCL single crystals is low under TEM observation in contrast to that in the thin film sample of PCL homopolymers, revealing the PCL single crystals with low crystallinity in the entire thin film sample. After solvent annealing by toluene vapor for 15 min, the as-spun PCL single crystal disappears and the flat-on PLLA single crystal is observed (Figure 6a). In accordance with the solubility parameters of toluene [8.9 $(cal/cm^3)^{0.5}$], PEO [9.9 (cal/

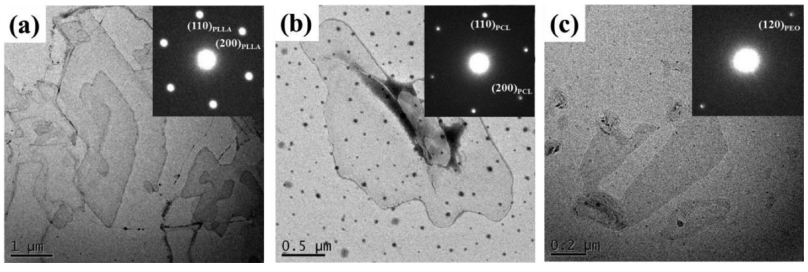

Figure 5. TEM micrographs and the corresponding SAED patterns of the PEO5-PCL3-PLLA6 thin films after melt crystallization at (a) 90, (b) 45, and (c) −10 °C for 3 h.

DOI: 10.1021/acs.macromol.5b02042
Macromolecules 2015, 48, 8526−8533

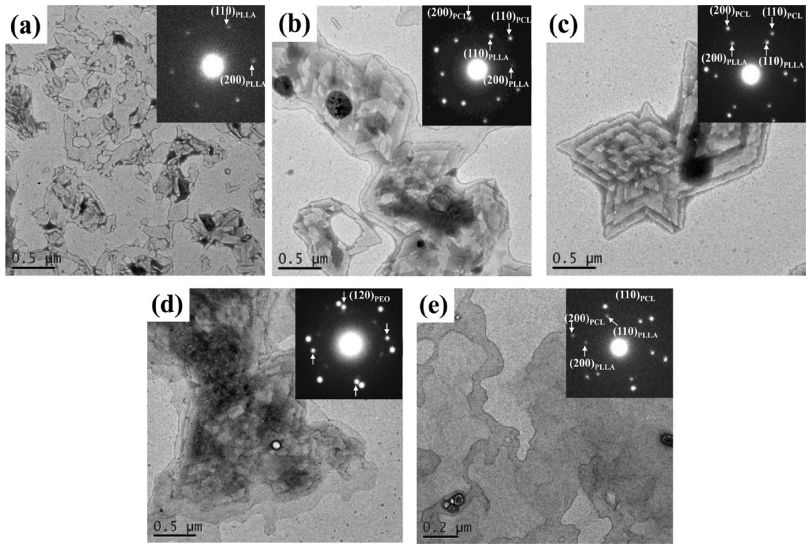

Figure 6. A series of TEM micrographs of the PEO5-PCL3-PLLA6 thin films after solvent annealing by toluene vapor for (a) 15, (b) 30, (c) 60, (d) 180, and (e) 360 min. The insets are the corresponding SAED patterns.

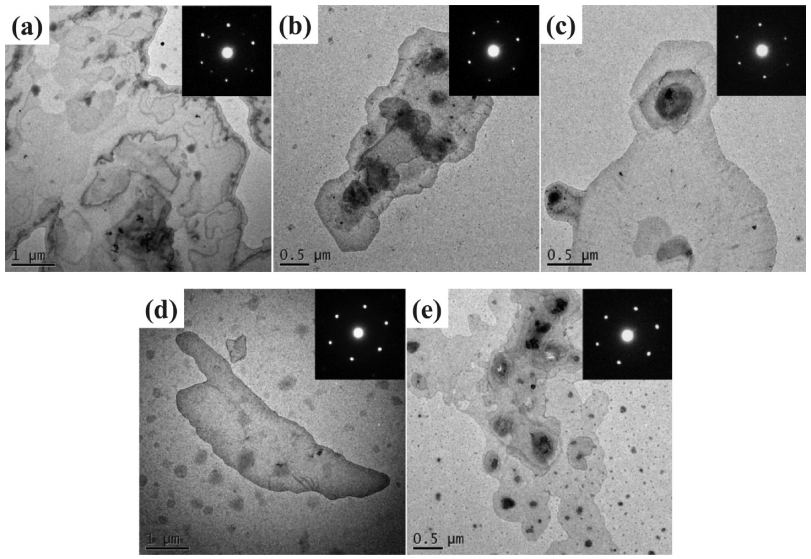

Figure 7. A series of TEM micrographs of the PEO5-PCL3-PLLA1 thin films after solvent annealing by toluene vapor for (a) 15, (b) 30, (c) 60, (d) 180, and (e) 360 min.

$cm^3)^{0.5}$], PCL [9.4 (cal/$cm^3)^{0.5}$], and PLLA [10.9 (cal/$cm^3)^{0.5}$],[49] toluene is regarded as a good solvent for the PCL block. Therefore, the disappearance of the as-spun PCL crystals is attributed to the dissolution by toluene vapor. Inversely, the poor solubility of toluene toward the PLLA block gives rise to the aggregations of the PLLA block chains, which can play as nuclei for the crystal growth. Consequently, the first-crystallized PLLA single crystal was obtained. With increasing the annealing time to 30 min, the well-defined crystal with lozenge shape can be observed (Figure 6b). The corresponding SAED pattern reveals 12 reflections resulted from the [001] zonal reflections of the PCL and PLLA crystals including the $(200)_{PLLA}$, $(110)_{PLLA}$, $(200)_{PCL}$, and $(110)_{PCL}$ reflections (inset in Figure 6b). This indicates the coexistence of the flat-on PLLA and PCL crystals, namely, dual-layered PLLA/PCL single crystals. This is consistent with the TEM micrograph revealing small PCL crystals on a PLLA-based crystal. We suggest that the formation of the double-crystalline layered crystal is dependent upon the constituent sequence of the blocks. The first-crystallized PLLA single crystals may drive the exclusion of the amorphous PCL and PEO block chains onto the crystal surfaces. Owing to lower nucleation barrier, the adjacent PCL chains subsequently crystallize prior to the terminated PEO blocks. Accordingly, the PCL crystals on a PLLA-based crystal can be obtained. In Figure 6c, after fuming for 60 min, the dual-layered PLLA/PCL single crystal becomes larger and more perfect. Most interestingly, after solvent annealing by toluene for 180 min, the crystalline morphology with 16 reflections is observed (Figure 6d). Except for the 12 reflections from the [001] zonal reflections of the PCL and PLLA crystals, four $(120)_{PEO}$ reflections (arrows in the inset of Figure 6d) are observed. This reveals the formation of the triple-crystalline crystal with flat-on chain orientation, that is, a trilayered PLLA/PCL/PEO single crystal. The specific morphological evolution is consistent with the results from the Pt-shadowed PEO5-PCL3-PLLA6 thin films (Figure S9). To the best of our

DOI: 10.1021/acs.macromol.5b02042
Macromolecules 2015, 48, 8526−8533

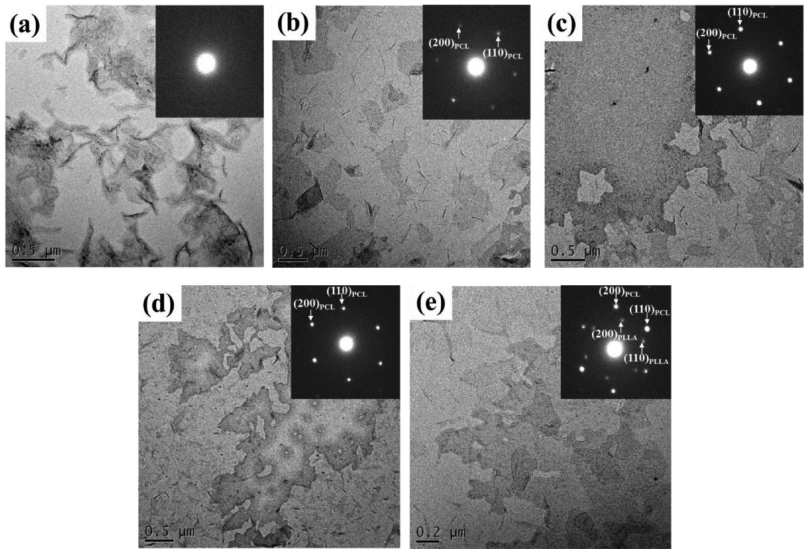

Figure 8. A series of TEM micrographs of the PEO5-PCL3-PLLA6 thin films after solvent annealing by *n*-hexanol vapor for (a) 15, (b) 30, (c) 60, (d) 180, and (e) 360 min. The insets are the corresponding SAED patterns.

knowledge, this is the first report of a triple-crystalline thin film crystal with flat-on chain orientation. However, after annealing for 360 min, the third-crystallized PEO is dissolved by toluene vapor. Accordingly, the reversion to the double-crystalline PLLA/PCL crystal is found (Figure 6e).

To investigate the effect of the PLLA chain length on the crystal growth in thin film, the PEO5-PCL3-PLLA1 thin films were treated by the same solvent annealing process (Figure 7). After toluene annealing for 15 min, the single crystals having ten reflections comprising of the inner four $(120)_{PEO}$ and outer six $(200)_{PCL}$ and $(110)_{PCL}$ reflections can be observed (Figures 7a), indicating the formation of the dual-layered PCL/PEO crystals with flat-on orientation. Because of the noncrystalline PLLA in the PEO5-PCL3-PLLA1, the PCL block first crystallized and the PEO crystallization was subsequently adhered to slide the sequential crystallization forward as compared with that in the PEO5-PCL3-PLLA6. With the extension of the annealing time to 30 min, the preformed PEO crystal is dissolved, and only flat-on PCL single crystal remains (Figures 7b). The dissolution of the PEO crystal is similar to that in the PEO5-PCL3-PLLA6 after toluene annealing for 360 min. With increasing the annealing time to 60, 180, and 360 min (Figures 7c–e), no further change for the crystalline texture is obtained. In this study, the PEO5-PCL3-PLLA1 with short chain length of the PLLA block was originally designed to explore the possibility to acquire the PLLA single crystal with fully extended chain conformation. However, owing to the weak crystallization force and high compatibility with the adjacent PCL block, the PLLA block exhibits noncrystallizable feature in the PEO5-PCL3-PLLA1 even though the solvent-induced crystallization was utilized. Also, because of the noncrystalline PLLA, the crystal growths of PCL and PEO blocks accelerate significantly in the PEO5-PCL3-PLLA1 in contrast to the PEO5-PCL3-PLLA6.

To manipulate of the sequence of the crystal growth, we utilized a polar solvent, *n*-hexanol, for solvent annealing. After fuming by *n*-hexanol vapor for 15 min, the noncrystalline morphology is obtained (Figure 8a) due to the dissolution of the as-spun imperfect PCL crystals. Interestingly, the flat-on PCL single crystal appears after solvent annealing for 30 min (Figure 8b). The formation of the featureless PCL single crystals might be due to the confinement effect of the centered PCL block by the adjacent PLLA and PEO blocks. Similar flat-on PCL single crystals can be found after the solvent annealing for 60 and 180 min (Figures 8c,d). Notably, after fuming for 360 min, the SAED pattern reveals 12 reflections belonging to the coexistence of the [001] zonal reflections of the PCL and PLLA crystals (inset in Figure 8e). This indicates the formation of the dual-layered PCL/PLLA single crystal. Similar results can be obtained in the Pt-shadowed thin films (Figure S10). According to the solubility parameter of *n*-hexanol [10.7 $(cal/cm^3)^{0.5}$],[49] *n*-hexanol should be regarded as a selective solvent for the PLLA block. However, owing to strong polarity, *n*-hexanol, in principle, is generally regarded as a selective solvent for PEO. Accordingly, the poor solubility of the *n*-hexanol toward the PCL block may first drive the formation of the PCL single crystals in the early stage. The PLLA block subsequently crystallized to form dual-layered PCL/PLLA crystal. With the continued increase of the annealing time, the double-crystalline texture remained unchanged, revealing the noncrystalline PEO in the *n*-hexanol-annealed PEO-PCL-PLLA thin films. This is attributed to the excellent solubility of *n*-hexanol toward the PEO block chains. Different from the PEO5-PCL3-PLLA6, only flat-on PCL single crystals can be found in the PEO5-PCL3-PLLA1 thin films after solvent annealing by *n*-hexanol (Figure S11) due to the noncrystalline PLLA block. As a result, the crystallization sequence of the layer-by-layer crystal growth can be controlled by solvent selectivity in the triple-crystalline BCP thin film.

We also found specific epitaxial growth in the triple-crystalline PEO-PCL-PLLA BCP thin film. As analyzed in Figure 9a, the first case represents that the angle enclosed by the a_{PCL} and a_{PLLA} is zero ($\phi = 0°$) in the double-crystalline PLLA/PCL crystals (Figures 6c,e). Based on the lattice parameters of the PCL and the PLLA crystals, 2 times of a_{PLLA} is approximately equal to 3 times of a_{PCL}, revealing the corresponding lattice mismatch of 4.5%. Also, the angle $\phi = 30°$ enclosed by the a_{PLLA} and a_{PCL} can be obtained in the second case (Figure 6b). This reveals that the growth plane of the $(010)_{PCL}$ is parallel to the $(110)_{PLLA}$ with the lattice mismatch of 4.2% (Figure 9b). Accordingly, this expresses the result that the second-crystallized PCL exhibits the epitaxial growth with

DOI: 10.1021/acs.macromol.5b02042
Macromolecules 2015, 48, 8526–8533

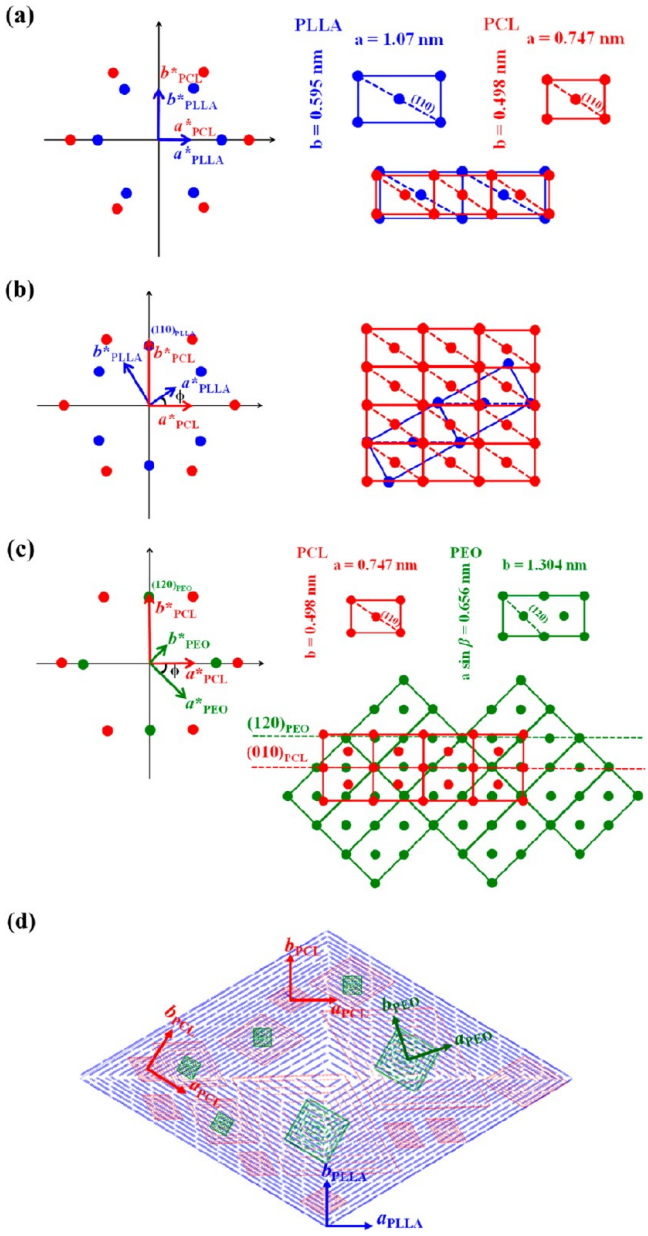

Figure 9. Illustrations of lattice matching viewing along *c* direction for the PLLA (blue), PCL (red), and PEO (green) crystals with (a) ϕ = 0°, (b) ϕ = 30°, and (c) ϕ = 45°. (d) Morphological geometry of the triple-crystalline layered crystals.

the first-crystallized PLLA in the dual-layered PLLA/PCL crystal. The dual-layered PCL/PLLA crystal in the *n*-hexanol system also reveals the epitaxial growth of ϕ = 30°, indicating the mutual epitaxy between the PCL and PLLA crystals despite the crystalline sequence. Moreover, the third-crystallized PEO crystal also epitaxially grows with respect to the second-crystallized PCL (Figure 6d). As shown in Figure 9c, the growth plane of $(120)_{PEO}$ is parallel to the $(010)_{PCL}$ (ϕ = 45° enclosed by the a_{PCL} and a_{PEO}). Figure 9d shows the morphological illustration of the triple-crystalline crystals by solvent-induced crystallization. As shown, the epitaxial growth of the third-crystallized PEO and second-crystallized PCL block chains on a leading PLLA-based single crystal is carried out, revealing the layer-by-layer triple-crystalline crystal of the BCP thin film. Consequently, the epitaxial growths among the layered crystals reveal that the triple-crystalline layer-by-layer single crystals can be induced by the specific folding surface of the leading crystal having low surface energy for the subsequent crystal growth.

CONCLUSIONS

The absence of the multiple-crystalline morphologies in the melt-crystallized thin films is due to the confinement effect by the robust first-crystallized single crystals. In contrast, multiple-crystalline textures of the PEO-PCL-PLLA BCP thin films can be manipulated by the control of the polymer/solvent interaction and fuming time. A unique morphological evolution from single to double and to triple crystallization (PLLA → PCL → PEO) in sequence is observed using toluene for solvent annealing. With solvent annealing by *n*-hexanol, the different sequential growth, i.e., PCL → PLLA, is obtained. The noncrystalline PEO is attributed to the good solubility of *n*-hexanol toward PEO. We also found that the first-crystallized PLLA can serve as a crystalline substrate to induce epitaxial growth of the second-crystallined PCL. Moreover, the $(120)_{PEO}$ of the third-crystallized PEO subsequently grows epitaxially with the $(010)_{PCL}$ to form the trilayered single crystal. As a result, the evolution from single- to dual- and to trilayered single crystals exhibits layer-by-layer epitaxial growth in sequence. This can provide a novel concept to fabricate trilayered biocompatible single crystals in thin film. Also, the folding direction or topography of the multilayered single crystals can be manipulated by using the preferred polymer single crystal as a fundamental template.

ASSOCIATED CONTENT

Supporting Information

The Supporting Information is available free of charge on the ACS Publications website at DOI: 10.1021/acs.macromol.5b02042.

WAXD profiles of the PEO5-PCL3-PLLA1 and PEO5-PCL3-PLLA6 after slow cooling from melt and after quenched from the melt, TEM micrographs, and the corresponding SAED patterns of the PEO5-PCL3-PLLA6 thin films after two- and three-step crystallization, TEM micrograph and the corresponding SAED pattern of the as-spun PEO5-PCL3-PLLA6 thin film from chlorobenzene solution (0.5 wt %), a series of TEM micrographs of the Pt-shadowed PEO5-PCL3-PLLA6 thin films after solvent annealing by toluene and *n*-hexanol vapors for various time periods, a series of TEM micrographs of the PEO5-PCL3-PLLA1 thin films after solvent annealing by *n*-hexanol vapor for various time periods (PDF)

AUTHOR INFORMATION

Corresponding Author

*Tel +886-7-5252000; Fax +886-5-5254099; e-mail ywchiang@mail.nsysu.edu.tw (Y.-W.C.).

Notes

The authors declare no competing financial interest.

ACKNOWLEDGMENTS

Authors thank Mr. Hsien-Tsan Lin of Regional Instruments Center at National Sun Yat-Sen University for his help in TEM experiments. We also thank Drs. U.-S. Jeng and C.-J. Su of National Synchrotron Radiation Research Center (Taiwan) for

DOI: 10.1021/acs.macromol.5b02042
Macromolecules 2015, 48, 8526−8533

their help in synchrotron WAXD experiments. Authors appreciate the Ministry of Science and Technology of the Republic of China (MOST 104-2221-E-110-073), Taiwan, for financially supporting this research.

REFERENCES

(1) Kumar, N.; Ravikumar, M. N.; Domb, A. J. *Adv. Drug Delivery Rev.* **2001**, *53*, 23−44.
(2) Panday, A.; Mullin, S.; Gomez, E. D.; Wanakule, N.; Chen, V. L.; Hexemer, A.; Pople, J.; Balsara, N. P. *Macromolecules* **2009**, *42*, 4632−4637.
(3) Birnkrant, M. J.; Li, C. Y.; Natarajan, L. V.; Tondiglia, V. P.; Sutherland, R. L.; Bunning, T. J. *Soft Matter* **2011**, *7*, 4729−4734.
(4) Yang, C. S.; Wu, H. C.; Sun, J. S.; Hsiao, H. M.; Wang, T. W. *ACS Appl. Mater. Interfaces* **2013**, *5*, 10985−10994.
(5) Baghgar, M.; Barnes, A. M.; Pentzer, E.; Wise, A. J.; Hammer, B. A. G.; Emrick, T.; Dinsmore, A. D.; Barnes, M. D. *ACS Nano* **2014**, *8*, 8344−8349.
(6) Chiang, Y. W.; Huang, Y. W.; Huang, S. H.; Huang, P. S.; Mao, Y. C.; Tsai, C. K.; Kang, C. S.; Tsai, J. C.; Su, C. J.; Jeng, U. S.; Tseng, W. H. *J. Phys. Chem. C* **2014**, *118*, 19402−19414.
(7) Chen, W. Y.; Li, C. Y.; Zheng, J. X.; Huang, P.; Zhu, L.; Ge, Q.; Quirk, R. P.; Lotz, B.; Deng, L.; Wu, C.; Thomas, E. L.; Cheng, S. Z. D. *Macromolecules* **2004**, *37*, 5292−5299.
(8) Zheng, J. X.; Xiong, H.; Chen, W. Y.; Lee, K.; Van Horn, R. M.; Quirk, R. P.; Lotz, B.; Thomas, E. L.; Shi, A. C.; Cheng, S. Z. D. *Macromolecules* **2006**, *39*, 641−650.
(9) Chao, C. C.; Chen, C. K.; Chiang, Y. W.; Ho, R. M. *Macromolecules* **2008**, *41*, 3949−3956.
(10) Hsiao, M. S.; Chen, W. Y.; Zheng, J. X.; Van Horn, R. M.; Quirk, R. P.; Ivanov, D. A.; Thomas, E. L.; Lotz, B.; Cheng, S. Z. D. *Macromolecules* **2008**, *41*, 4794−4801.
(11) Chiang, Y. W.; Ho, R. M.; Thomas, E. L.; Burger, C.; Hsiao, B. S. *Adv. Funct. Mater.* **2009**, *19*, 448−459.
(12) Hsiao, M. S.; Zheng, J. X.; Van Horn, R. M.; Quirk, R. P.; Thomas, E. L.; Chen, H. L.; Lotz, B.; Cheng, S. Z. D. *Macromolecules* **2009**, *42*, 8343−8352.
(13) Su, M.; Huang, H.; Ma, X.; Wang, Q.; Su, Z. *Macromol. Rapid Commun.* **2013**, *34*, 1067−1071.
(14) Reiter, G. *Chem. Soc. Rev.* **2014**, *43*, 2055−2065.
(15) Takeshita, H.; Shiomi, T.; Takenaka, K.; Arai, F. *Polymer* **2013**, *54*, 4776−4789.
(16) Nakagawa, S.; Marubayashi, H.; Nojima, S. *Eur. Polym. J.* **2015**, *70*, 262−275.
(17) Li, B.; Li, C. Y. *J. Am. Chem. Soc.* **2007**, *129*, 12−13.
(18) Wang, B.; Li, B.; Ferrier, R. C. M.; Li, C. Y. *Macromol. Rapid Commun.* **2010**, *31*, 169−175.
(19) Chen, X.; Dong, B.; Wang, B.; Shah, R.; Li, C. Y. *Macromolecules* **2010**, *43*, 9918−9927.
(20) Huang, S.; Jiang, S. *RSC Adv.* **2014**, *4*, 24566−24583.
(21) He, C.; Sun, J.; Zhao, T.; Hong, Z.; Zhuang, X.; Chen, X.; Jing, X. *Biomacromolecules* **2006**, *7*, 252−258.
(22) He, C.; Sun, J.; Ma, J.; Chen, X.; Jing, X. *Biomacromolecules* **2006**, *7*, 3482−3489.
(23) Van Horn, R. M.; Zheng, J. X.; Sun, H. J.; Hsiao, M. S.; Zhang, W. B.; Dong, X. H.; Xu, J.; Thomas, E. L.; Lotz, B.; Cheng, S. Z. D. *Macromolecules* **2010**, *43*, 6113−6119.
(24) Hamley, I. W.; Castelletto, V.; Castillo, R. V.; Müller, A. J.; Martin, C. M.; Pollet, E.; Dubois, P. *Macromolecules* **2005**, *38*, 463−472.
(25) Castillo, R. V.; Müller, A. J.; Raquez, J. M.; Dubois, P. *Macromolecules* **2010**, *43*, 4149−4160.
(26) Casas, M. T.; Puiggalí, J.; Raquez, J. M.; Dubois, P.; Córdova, M. E.; Müller, A. J. *Polymer* **2011**, *52*, 5166−5177.
(27) Peponi, L.; Navarro-Baena, I.; Báez, J. E.; Kenny, J. M.; Marcos-Fernández, A. *Polymer* **2012**, *53*, 4561−4568.
(28) Sun, J.; Hong, Z.; Yang, L.; Tang, Z.; Chen, X.; Jing, X. *Polymer* **2004**, *45*, 5969−5977.
(29) Yang, J.; Zhao, T.; Zhou, Y.; Liu, L.; Li, G.; Zhou, E.; Chen, X. *Macromolecules* **2007**, *40*, 2791−2797.
(30) Huang, S.; Jiang, S.; An, L.; Chen, X. *J. Polym. Sci., Part B: Polym. Phys.* **2008**, *46*, 1400−1411.
(31) Albuerne, J.; Marquez, L.; Müller, A. J.; Raquez, J. M.; Degée, P.; Dubois, P.; Castelletto, V.; Hamley, I. W. *Macromolecules* **2003**, *36*, 1633−1644.
(32) Müller, A. J.; Albuerne, J.; Marquez, L.; Raquez, J. M.; Degée, P.; Dubois, P.; Hobbs, J.; Hamley, I. W. *Faraday Discuss.* **2005**, *128*, 231−252.
(33) Zhou, S.; Deng, X.; Yang, H. *Biomaterials* **2003**, *24*, 3563−3570.
(34) Gaucher, G.; Dufresne, M. H.; Sant, V. P.; Kang, N.; Maysinger, D.; Leroux, J. C. *J. Controlled Release* **2005**, *109*, 169−188.
(35) Mahmud, A.; Xiong, X. B.; Lavasanifar, A. *Macromolecules* **2006**, *39*, 9419−9428.
(36) Savva, I.; Odysseos, A. D.; Evaggelou, L.; Marinica, O.; Vasile, E.; Vekas, L.; Sarigiannis, Y.; Krasia-Christoforou, T. *Biomacromolecules* **2013**, *14*, 4436−4446.
(37) He, W.-N.; Xu, J.-T. *Prog. Polym. Sci.* **2012**, *37*, 1350−1400.
(38) Wang, Y.; Chen, J.; Li, S.; Su, Q.; Wang, J.; Yang, X. *Macromolecules* **2011**, *44*, 1737−1741.
(39) Vivas, M.; Contreras, J.; López-Carrasquero, F.; Lorenzo, A. T.; Arnal, M. L.; Balsamo, V.; Müller, A. J.; Laredo, E.; Schmalz, H.; Abetz, V. *Macromol. Symp.* **2006**, *239*, 58−67.
(40) Liu, C. C.; Chu, W. C.; Li, J. G.; Kuo, S. W. *Macromolecules* **2014**, *47*, 6389−6400.
(41) Takahashi, Y.; Tadokoro, H. *Macromolecules* **1973**, *6*, 672−675.
(42) Nakagawa, S.; Kadena, K. I.; Ishizone, T.; Nojima, S.; Shimizu, T.; Yamaguchi, K.; Nakahama, S. *Macromolecules* **2012**, *45*, 1892−1900.
(43) Yang, J.; Liang, Y.; Luo, J.; Zhao, C.; Han, C. C. *Macromolecules* **2012**, *45*, 4254−4261.
(44) Takahashi, Y.; Tadokoro, H. *Macromolecules* **1973**, *6*, 672−675.
(45) Chatani, Y.; Okita, Y.; Tadokoro, H.; Yamashita, Y. *Polym. J.* **1970**, *1*, 555−562.
(46) Hoogsteen, W.; Postema, A. R.; Pennings, A. J.; Ten Brinke, G.; Zugenmaier, P. *Macromolecules* **1990**, *23*, 634−642.
(47) Cartier, L.; Okihara, T.; Ikada, Y.; Tsuji, H.; Puiggali, J.; Lotz, B. *Polymer* **2000**, *41*, 8909−8919.
(48) Zhu, L.; Cheng, S. Z. D.; Calhoun, B. H.; Ge, Q.; Quirk, R. P.; Thomas, E. L.; Hsiao, B. S.; Yeh, F.; Lotz, B. *J. Am. Chem. Soc.* **2000**, *122*, 5957−5967.
(49) Du, Y.; Xue, Y.; Frisch, H. L. *Physical Properties of Polymers Handbook*, Mark, J. E., Ed.; AIP Press: New York, 1996; pp 227−240.

DOI: 10.1021/acs.macromol.5b02042
Macromolecules 2015, 48, 8526−8533